energies

MDPI

Article

Investigation on Induced Energy Extraction from High-Voltage Transmission Lines Based on Three-Coil WPT Systems

Weilong Li [1], Yuhang Chen [2,*], Zhou Peng [2], Xirui Wang [2] and Chenyang Xia [2]

[1] Anhui Academy of Coal Science, Hefei 230001, China
[2] School of Electrical Engineering, China University of Mining and Technology, Xuzhou 221008, China
* Correspondence: ts22230006a31ld@cumt.edu.cn

Abstract: In order to realize an online power supply, this article develops an explicit design of induction power extraction technology combined with wireless power transmission (WPT) technology. Unlike the power supply mode of traditional batteries of online monitoring devices of high-voltage transmission lines, this technology solves the short battery life cycle problems. First, the principle of induction power extraction is analyzed. Based on the equivalent circuit of the mutual inductance model, expressions of induction power extraction without and with core saturation are derived, respectively. According to the current transformer (CT) magnetic coupling diagram, the open-circuit voltage of the secondary side of the CT is deduced. Therefore, the CT material and size could be selected. The CT coupling model is used to equivalent the current transformer to the ideal voltage source. Then, the four basic topological spaces of the magnetic coupling resonant WPT system are analyzed and calculated, and the efficiency of the SS topology WPT system is analyzed. Furthermore, aiming at long-distance power transmission, this article described the building of a three-coil WPT system and the analysis of the corresponding transmission efficiency and output power expression. With the aid of Maxwell, the technology proposed is simulated based on a 110 kV high-voltage transmission line with 1.2 m as the transmission distance of the system. Finally, the influence of a coupling coefficient and load resistance on the transmission characteristics of the multicoil system is obtained. Consequently, the simulation results with a system output power of 14.4 W verify the effectiveness of the technology.

Keywords: induction power extraction; online monitoring; high-voltage transmission lines; wireless power transmission; three-coil

Citation: Li, W.; Chen, Y.; Peng, Z.; Wang, X.; Xia, C. Investigation on Induced Energy Extraction from High-Voltage Transmission Lines Based on Three-Coil WPT Systems. *Energies* **2023**, *16*, 3079. https://doi.org/10.3390/en16073079

Academic Editor: Pawel Rozga

Received: 3 March 2023
Revised: 23 March 2023
Accepted: 27 March 2023
Published: 28 March 2023

1. Introduction

1.1. Motivation and Incitement

With the development of the national economy, the demand for electricity and electricity quality has risen sharply, with the national power industry having been developed in-depth. High-voltage, extra-high-voltage, and even ultra-high-voltage transmission lines have been implemented across the north and south of China [1]. With the continuous improvement of the voltage level of transmission lines, the requirements of stability, safety, and reliability of transmission and distribution network systems have gradually increased. In recent years, emerging technologies, such as smart grids and distribution automation, have continuously emerged and are being promoted [2]. Improving the safety and stability of power transmission and improving power quality could further promote the development of these technologies.

The high-voltage transmission line is a complex energy network, which includes several parts, such as transelectric insulator strings, various connection fittings, transmission towers, and power wire materials. They are usually exposed to fields, where geographical and climatic environments are complex and variable, especially in mountainous, landslide,

and flood-prone areas, as well as extremely severe weather, such as ice, snow, and thunderstorms. In addition, they are widely distributed and have long line distances. Hence, a high-voltage transmission line can be easily damaged. Once a fault occurs in a certain part of the line, it can lead to a series of chain reactions, and even lead to a partial or entire power grid paralysis, bringing large losses to the national economy.

Online monitoring devices have been widely used in the state monitoring and fault diagnosis of transmission lines to provide timely feedback on the state information of transmission lines, preventing catastrophic accidents [3]. However, with the popularity of online monitoring technology, the power supply problem of online monitoring devices has become one of the most important problems requiring solving [4]. Due to geographical and self-insulation constraints, the power supply of high-voltage transmission lines cannot be transmitted directly from the high-voltage side to the low-voltage side through cables [5]. Therefore, the power supply problem of high-voltage line online monitoring devices, especially monitoring devices installed on transmission towers, has once again become a key bottleneck to the in-depth and mature development of smart grids [6].

In addition, since online monitoring devices for high-voltage transmission lines work under the malignant conditions of ultra-high potential and strong magnetic radiation, this means that higher requirements for the safety and reliability of its power supply are needed. Therefore, the development of a power supply that can work stably in fields for a long time is a prerequisite to ensure the reliable operation of transmission line online monitoring devices, and it is also the primary problem that should be solved to ensure that online monitoring technology can be integrated into the tide of smart grids.

1.2. Literature Review

At present, research on the power supply mode of online monitoring devices at home and abroad mainly includes the following:

1. Solar power: It collects photovoltaic energy mainly through solar cell arrays, and, at the same time, for online monitoring devices and battery power supplies. However, solar cells are susceptible to weather conditions, and the storage capacity in solar power systems is unlikely to be too large when it is cloudy and rainy for many days; hence, solar power systems may not be able to meet the power needs of online monitoring devices [7].
2. Laser power: At the low-voltage side, high-power laser generators are used to send light energy to the high-voltage side, and at the high-voltage side, photocells are used to convert light energy into electricity, which supplies power to high-voltage lines [8]. However, due to the large size of the transmitting and receiving devices and the fact that online detection equipment is usually installed on high-voltage lines, it is difficult to install power supply equipment, and the cost of its operation and maintenance is high.
3. Ultrasonic power supply: The utility model relates to an energy supply mode that uses ultrasonic waves as a medium to transmit electric energy. However, its equipment is expensive, and the conversion efficiency is low. Hence, it cannot be used on a large scale.
4. Microwave power: It is a means of transmitting energy in a vacuum or in the atmosphere without the aid of any other transmission lines. However, if a microwave power supply is applied to the power supply of online monitoring devices for high-voltage transmission lines, there is also a need to address the design and placement of receiving antennas, determining whether the microwave power supply can interfere with monitoring devices, and the issues surrounding operation and maintenance [9].

In order to optimize the real-time power supply for online monitoring devices of high-voltage transmission lines, this paper proposes a power supply mode combining current transformer power extraction technology and three-coil wireless power transmission (WPT) technology. Compared with the above four energy supply modes, the current transformer has the advantages of small size, low cost, high transmission power, and not being affected

by weather changes. In addition, the use of current transformer energy technology can avoid direct contact with energy sources and can solve the problem of insulation in the power supply [10–13]. In addition, compared with other wireless energy transmission technologies, the magnetic coupling resonant WPT technology has the advantages of a long transmission distance, high transmission power, high transmission efficiency, physical isolation, etc. [14,15]. The combination of CT induction power extraction technology and three-coil WPT technology can provide an appropriate solution to the problem of power supply insulation for online monitoring devices of high-voltage transmission lines [16].

In [4], according to the limitation of the plant application of induction energy harvesting devices for high-voltage transmission lines, several power supply modes are compared and the power supply mode of solar panels and accumulators is put forward. In order to deal with bad situations after magnetic saturation, silicon steel sheets with high-saturation permeability and low cost are used as the core material. In [5], based on the method of obtaining electricity through CT induction acquisition technology, a device for obtaining electricity is designed. The output power reaches 3 W. Two kinds of output voltage grades are provided. The maximum output current can reach 250 mA, and the utility model solves the power supply problem of the equipment in the power tunnel. In [6], a simple model of self-supply power is designed based on the analysis of circuit structure and take-up coil by using the principle of CT induction acquisition technology taking-up power for power overhead lines; the take-up power is approximately 5 W and is applied to the fault detection of high-voltage transmission lines.

At present, research surrounding power supply methods for online detection equipment based on the combination of CT induction power extraction technology and three-coil WPT technology is in the initial stages. There are still some problems, such as limitations in the transmission distance and the insufficient antisaturation ability of the magnetic core, leading to a high degree of magnetic saturation.

1.3. Contribution and Paper Organization

This paper presents an induction power extraction and three-coil WPT technology for high-voltage transmission lines. In this paper, the structure parameters of the CT ring are analyzed and the influence of the coil parameters on the energy efficiency of the magnetic coupling WPT system is analyzed. Based on this, this paper optimizes the structural and coil parameters of the CT ring, finally making the system have a larger induced voltage in the energy-fetching link. At the same time, the system has a longer transmission distance, improved size and cost of the equipment, and improved stability and practicability.

This paper first analyzes the principle of inductive energy acquisition and the principle of the magnetic coupling resonance wireless power transmission, which provides a theoretical basis for the proposal of the new method. Then, through the analysis and calculation of the influence of each structural parameter, the optimal parameter is selected and verified through a simulation. Finally, a three-coil CT inductive energy acquisition system with a longer transmission distance and a larger induced energy acquisition voltage is obtained.

2. Theoretical Analysis and Design of Induction Power Extraction

2.1. Analysis of CT Ring Induction Power Extraction

A CT-type induction power extraction model was adopted for the induction power extraction of high-voltage transmission lines. The current transformer was composed of a high-voltage transmission line on the primary side, a core, and a secondary winding. The current transformer was based on the principle of electromagnetic induction. When the alternating current passes the primary side of the high-voltage transmission line, induced in the secondary side with the same phase, the amplitude is proportional to the number of turns [17]. The primary side current is not affected by the secondary side, and the secondary side current is not affected by the load, which is only related to the primary side current and the core and winding [18]. When establishing the mathematical model of CT induction

power extraction technology, the skin and temperature effects of the winding were ignored, and the hysteresis eddy current loss of the core was also ignored. The magnetic coupling model of the power extraction CT is shown in Figure 1. The primary side was controlled through an alternating current and only had one turn of winding on it. In Figure 1, φ_m is the main magnetic flux, φ_{1m} and φ_{2m} are the leakage fluxes of the primary and secondary winding, respectively, φ_1 and φ_2 are the main magnetic fluxes of the primary and secondary winding, respectively, i_1 and i_2 are the currents of the primary and secondary winding, respectively, N_1 and N_2 are the turns of the primary and secondary winding, respectively, and e_1 and e_2 are the potentials of the primary and secondary winding, respectively.

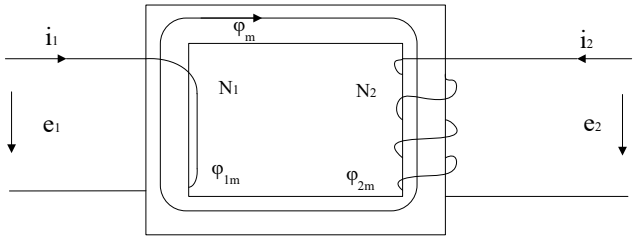

Figure 1. CT coupling relationship power extraction diagram.

The voltage effective value of the CT secondary side under no-load conditions was expressed as:

$$E_2 = \sqrt{2} \times 4.44 f N_2 \mu_0 \mu_r S \frac{I_1}{l} \quad (1)$$

where μ_r is the relative permeability of the magnetic core, μ_0 is the vacuum permeability, l is the effective magnetic circuit length, S is the cross-sectional area of the iron core, f is the frequency of the transmission line current, and I_1 is the effective value of the transmission line current.

2.2. Selection of CT Ring

For the selection of the CT ring, a larger initial permeability and a larger saturation permeability were necessary. The most commonly used iron core materials are nanocrystal, permalloy, and silicon steel [19]. The parameters of the three materials are listed in Table 1. It can be seen that the saturation magnetic induction intensity of silicon steel was large, and it was not easy to make the magnetic core enter a saturated state, while the magnetic permeability of the nanocrystal and permalloy was much larger than that of the silicon steel. Considering the economy and practicability of CT involved in this paper, silicon steel was selected as the core material of CT.

Table 1. Three core materials' basic parameters.

Basic Parameter	Silicon Steel	Permalloy	Nanocrystal
Saturation induction (B/H)	2.03	0.75	1.25
Initial permeability (μH/m)	10^2~10^3	(5~8) × 10^4	(5~10) × 10^4
Maximum permeability (μH/m)	4 × 10^4	60 × 10^4	60 × 10^4
Density (g/cm^3)	7.65	8.75	7.25
Packing fraction	0.95	0.9	0.7
Thickness (mm)	0.3	0.15	0.3

The core was designed to open the air gap to improve the maximum saturation magnetic induction intensity of the air gap and suppress the core saturation. In this case, the antisaturation characteristics and demagnetization ability of the iron core increased and the performance of the traditional current transformer was improved. At the same time, this structure of air gap also provided convenience for the installation of the current transformer on the high-voltage transmission line.

The relative permeability of the iron core in the case of an open-air gap could be derived as:

$$\mu_r = \frac{\mu_{Fe}}{\mu_{Fe}\frac{\delta}{l} + \frac{1}{\mu_{Fe}}} = \frac{1}{\frac{\delta}{l} + \frac{1}{\mu_{Fe}}} \approx \frac{\delta}{l} \tag{2}$$

2.3. Power Extraction of CT Ring

If the ring core of the current transformer was composed of a highly permeable material, it could be considered that the inductance of the primary and secondary sides of the current transformer was fully coupled, and the coupling coefficients of the primary and secondary sides were infinitely close to one. The current transformer was calculated using the mutual inductance model, and the equivalent circuit diagram is shown in Figure 2.

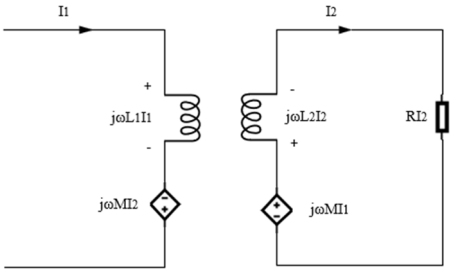

Figure 2. Current transformer equivalent circuit diagram.

Without considering the saturation of the core, the expression of the maximum power could be derived as:

$$P_{max} = \frac{(\omega^2 n^2 L_1^2\ \omega n^2 L_1)}{(2\omega^2 n^4 L_1^2) I_1^2} = \frac{1}{2}\omega L_1 I_1^2 \tag{3}$$

The above analysis of the maximum output power was based on an ideal state that the magnetic core was not saturated. In reality, the magnetic core would reach the saturation state with the increase in the primary side current. At this time, the current induced by the secondary side of the current transformer would be used for excitation, and significantly increasing the excitation current. The output current at the primary side would present with serious distortion, and the permeability of the magnetic core would also be significantly reduced, affecting the normal operation of the current transformer. If the equivalent resistance of the secondary side was not controlled to continuously increase to output higher power, it may lead to the saturation of the magnetic core. Therefore, it is necessary to calculate and discuss the state that may lead to core saturation.

The equivalent resistance of the secondary side could be adjusted to make the magnetic core not enter the saturated state when it was saturated. The maximum power output under the unsaturated state of the magnetic core was expressed as:

$$P_{max} = \frac{I_1^2}{\sqrt{(I_1^2 L_1^2)/(B_{max} S^2) - 1}} \omega L_1 \approx I_1 \cdot B_{max} S \omega \tag{4}$$

where B_{max} is the maximum magnetic induction intensity.

2.4. Power Extraction of CT Ring

The open-circuit voltage of the secondary side of the current transformer and the relative permeability of the iron core under the condition of an open-air gap could be calculated so that the current transformer could be equivalent to an ideal voltage source.

The parameters of the current transformer designed in this paper were given as follows: outer diameter R_0 = 44 mm; inner diameter R_i = 30 mm; width a = 30 mm; air gap δ = 1 mm; secondary side turns N_2 = 200; vacuum permeability $\mu_0 = 4\pi \times 10^{-7}$ H/m; system frequency f = 50 Hz.

By combining (1) and (2), the expression of the secondary open-circuit voltage after opening the air gap could be obtained as:

$$E_2 = \sqrt{2} \times 4.44 f N_2 \mu_0 S \frac{I_1}{\delta} \tag{5}$$

When the input voltage was 500 A, it could be concluded that the effective value of the open-circuit voltage on the secondary side of the current transformer was obtained as:

$$E_2 = 16.57 \text{ V} \tag{6}$$

Therefore, the current transformer could be equivalent to an AC voltage source with an amplitude of 1.414 E_2. It was shown that, when the current at the transmission terminal was 500 A, it was equivalent to a voltage source with an amplitude of 23.43 V.

3. Theoretical Analysis and Design of Magnetic Coupling Resonant WPT System

3.1. Mathematical Model of Magnetic Coupling Resonant Wireless Power Transmission System

According to the transmission coil and the receiving coil capacitor compensation, there were four basic compensation topological spaces for the magnetically coupled resonant WPT, as shown in Figure 3.

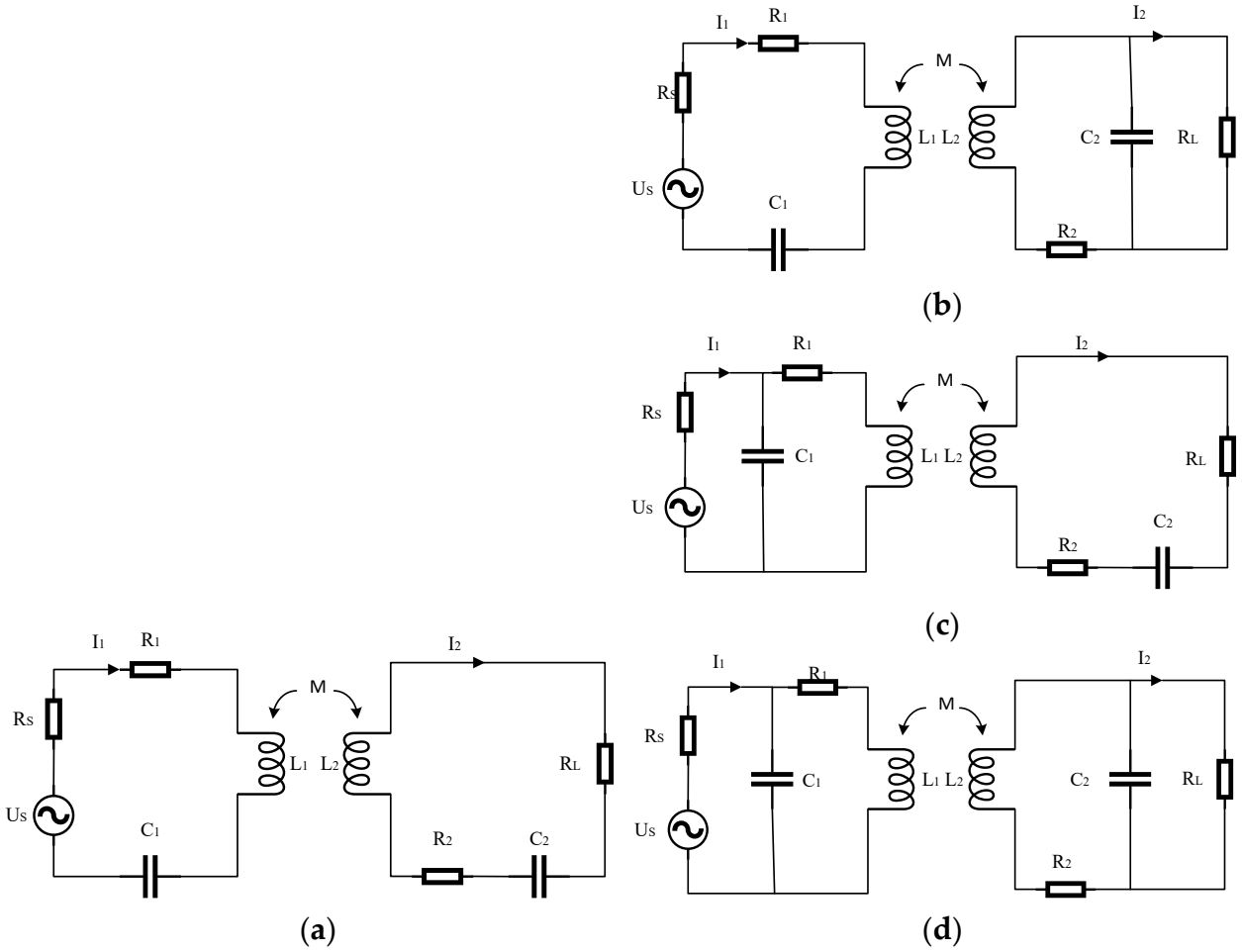

Figure 3. Equivalent circuit of topological structure: (**a**) SS topology structure; (**b**) SP topology structure; (**c**) PS topology structure; (**d**) PP topology structure.

Through the calculation of the four topological equivalent circuits, the output power, transmission efficiency, and compensation capacitance of the magnetic coupling resonant

wireless power transmission system under four structures could be obtained, as shown in Tables 2 and 3.

Table 2. Transmission characteristics of magnetically coupled resonant WPT.

Topological Structure	Output Power	Transmission Efficiency
SS	$\frac{(\omega M U_S)^2 R_L}{(Z_{11}Z_{21}+\omega^2M^2)^2}$	$\frac{\omega^2M^2R_L}{(Z_{11}Z_{21}+\omega^2M^2)Z_{21}}$
SP	$\frac{(\omega M U_S)^2 R_L}{(Z_{11}Z_{22}+\omega^2M^2)^2(1+j\omega C_2)}$	$\frac{\omega^2M^2R_L}{(Z_{11}Z_{22}+\omega^2M^2)(1+j\omega C_2R_L)}$
PS	$\frac{(\omega M U_S)^2 R_L}{(Z_{12}Z_{21}+\omega^2M^2)^2}$	$\frac{\omega^2M^2R_L}{(Z_{12}Z_{21}+\omega^2M^2)Z_{21}}$
PP	$\frac{(\omega M U_S)^2 R_L}{(Z_{12}Z_{22}+\omega^2M^2)^2(1+j\omega C_2)}$	$\frac{\omega^2M^2R_L}{(Z_{12}Z_{22}+\omega^2M^2)(1+j\omega C_2R_L)}$

Table 3. Compensation capacitance of magnetically coupled resonant WPT.

Topological Structure	Compensation Capacitor C_1	Compensation Capacitor C_2
SS	$\frac{1}{\omega^2L_1}$	$\frac{1}{\omega^2L_2}$
SP	$\frac{L_2}{\omega^2(L_1L_2-M^2)}$	$\frac{1}{\omega^2L_2}$
PS	$\frac{L_1R_L^2}{\omega^2L_1^2R_L^2+\omega^4M^4}$	$\frac{1}{\omega^2L_2}$
PP	$\frac{L_1L_2-M^2L_2^2}{\omega^2(L_1L_2-M^2)^2+\frac{M^4R_L^2}{L_2^2}}$	$\frac{1}{\omega^2L_2}$

It can be seen from Table 3 that the compensation capacitance of the transmitter was not affected by the load of the receiver, and it was only related to the system frequency and the self-inductance of the transmitter only in SS topology.

The transmission efficiency of the SS topology under resonant conditions could be obtained through the compensation capacitance expression.

$$\eta = \frac{(\omega^2M^2R_L)}{[R_1(R_2+R_L)+\omega^2M^2](R_2+R_L)} \tag{7}$$

Similarly, the transmission efficiency of the other three topological spaces could be obtained. It could be found from the expression that the transmission efficiency expressions of the SS and PS topological spaces were the same, and the transmission efficiency expressions of the SP and PP topological spaces were the same. Hence, the transmission efficiency was not related to the structure of the transmitter, but to the receiver.

It could be known from the principle of series resonance that the reactance of the primary side of the SS topology was zero in the resonant state. The current of the primary side was large and the voltage was small in the resonant state because of the small resistance value of the coil. The output current of the secondary side was constant. The output power and transmission efficiency mainly depended on the mutual inductance, resonant frequency, and load resistance of the coupling coil.

3.1.1. Relationships between Output Power, Transmission Efficiency, and Coil Mutual Inductance

The system frequency f was 100 kHZ, the input voltage was 100 V, the load resistance R_L was =10 Ω, and the coil resistance R was 0.5 Ω. The relationship between the transmission power and efficiency with mutual inductance is shown in Figures 4 and 5.

It can be seen from Figure 4 that the output power reached the maximum when the mutual inductance was close to 5 μH. It can be seen from Figure 5 that the transmission efficiency of the system tended to be stable and reached the maximum after the mutual inductance was 10 μH.

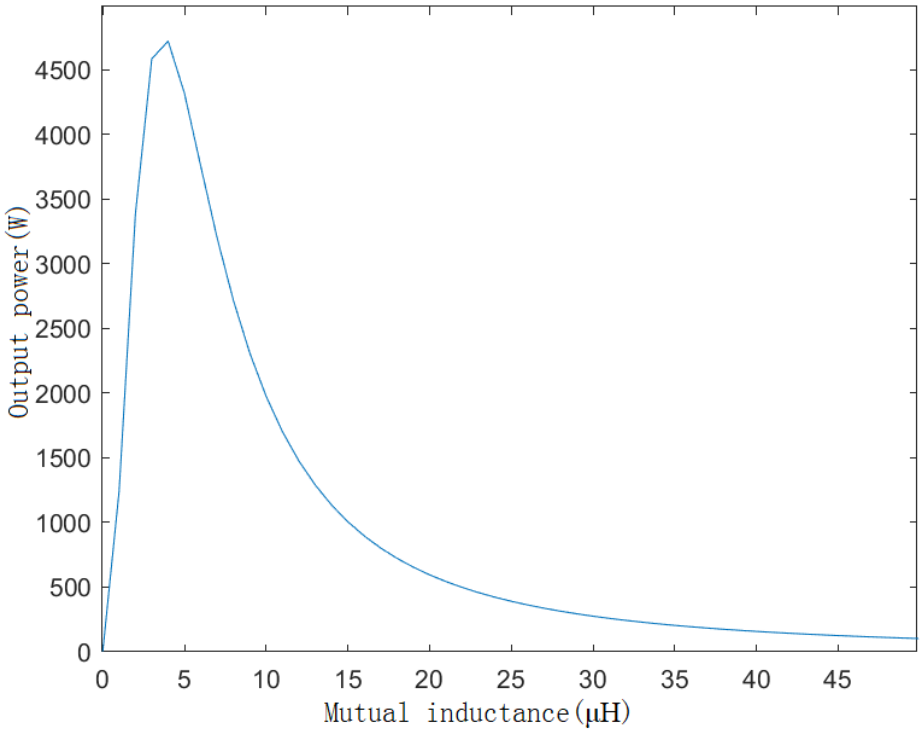

Figure 4. Relationship between output power and mutual inductance.

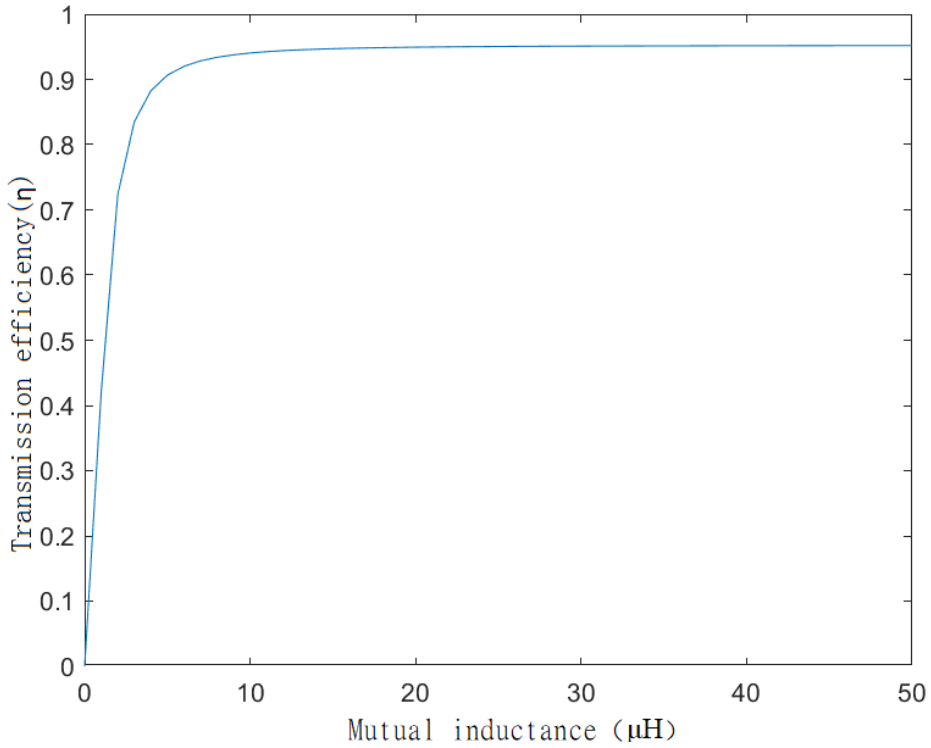

Figure 5. Relationship between transmission efficiency and mutual inductance.

3.1.2. Relationships between Output Power, Transmission Efficiency, and Load Resistance

When the system frequency f was 100 kHz, the input voltage was 100 V, the coil mutual inductance was M = 100 μH, the coil resistance R was 0.5 Ω, the relationship between the transmission power and efficiency of the system with the load resistance is shown in Figures 6 and 7.

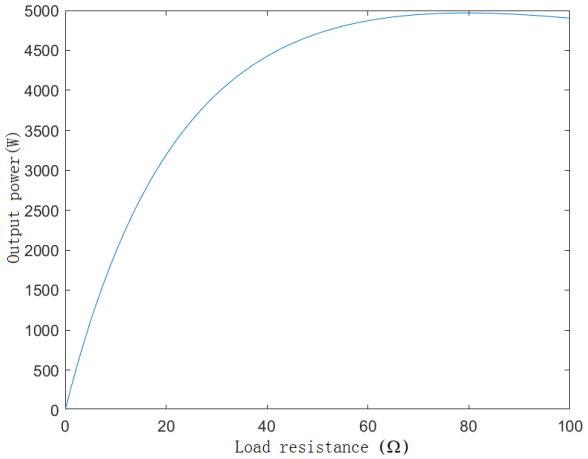

Figure 6. Relationship between output power and load resistance under the two coils.

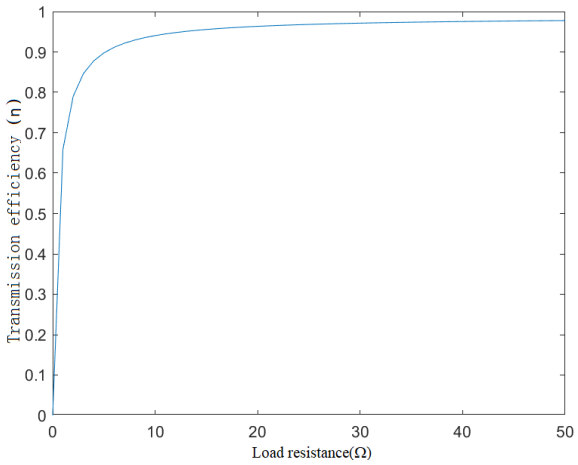

Figure 7. Relationship between transmission efficiency and load resistance under the two coils.

It can be seen from Figure 6 that the output power increased gradually with the increase in load resistance. As seen from Figure 7, the transmission efficiency tended to be stable when the load resistance was higher than 30 Ω.

3.2. Theoretical Analysis of Three-Coil Magnetic Coupling Resonant WPT System

The multicoil WPT could be used to improve the distance of the WPT. The three-coil magnetic coupling resonant WPT system contained three different coils, which were the transmission coil connected to the high-frequency power supply, the relay coil, and the receiving coil with a load. As shown in Figure 8, based on the mutual inductance theory, the equivalent circuit model of the system was established by using the SS topology structure.

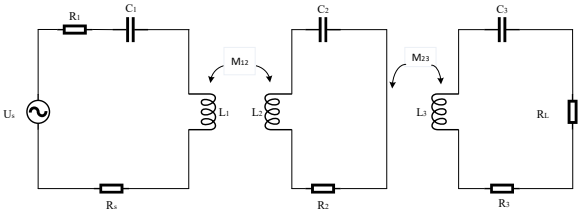

Figure 8. Three-coil magnetic coupling resonant wireless power transmission system circuit model.

In Figure 8, U_S is the high-frequency voltage, R_1, R_2, R_3, R_S, and R_L are the resistance of the transmitting coil, the resistance of the relay coil, the resistance of the receiving coil, the internal resistance of the power supply, and the resistance of the load, respectively; L_1,

L_2, and L_3 are three equivalent inductance values of the coil, and C_1, C_2, and C_3 are the capacitor compensations of the three coils.

The output power and transmission efficiency of the system could be obtained by listing the KVL equation of the circuit model when the system was in a resonant state.

$$P_{out} = {I_3}^2 R_L = \frac{(\omega^2 M_{12} M_{23})^2 U_S^2 R_L}{[(\omega M_{12})^2 (R_3 + R_L) + (R_S + R_1)[R_2(R_3 + R_L) + (\omega M_{23})^2]]^2} \quad (8)$$

$$\eta = \frac{(\omega {M_{12}}^2 {M_{23}}^2 R_L)}{(R_2(R_3 + R_L) + (\omega M_{23})^2)} \beta \quad (9)$$

$$\beta = \frac{1}{((\omega M_{12})^2 (R_3 + R_L) + (R_S + R_1)[R_2(R_3 + R_L) + (\omega M_{23})^2])} \quad (10)$$

3.3. Analysis of Influence Factors of Three-Coil Magnetic Coupling Resonant WPT System

3.3.1. Effect of Coupling Coefficient on Output Power

In the three-coil WPT system, the distance between the receiving coil and the transmitting coil was large and the mutual inductance could be ignored. Hence, only the mutual inductance between the adjacent coils was considered. By substituting the coupling coefficient formula into the output power expression, it had:

$$P_{out} = {I_3}^2 R_L = \frac{\omega^4 {k_{12}}^2 {k_{23}}^2 L^4 U_S^2 R_L}{[\omega^2 {k_{12}}^2 L^2 (R_3 + R_L) + (R_S + R_1)[R_2(R_3 + R_L) + \omega^2 {k_{12}}^2 L^2]]^2} \quad (11)$$

where frequency f = 100 kHz, input voltage U_S = 100 V, $R_1 = R_2 = R_3 = R$ = 0.5 Ω, and $L_1 = L_2 = L_3 = L$ = 297.08 μH. Ignoring the internal resistance of the input power supply R_S and making the load resistance value R_L = 15 Ω, based on these parameters, the relationship between the coupling coefficient and the output power could be obtained, as shown in Figure 9.

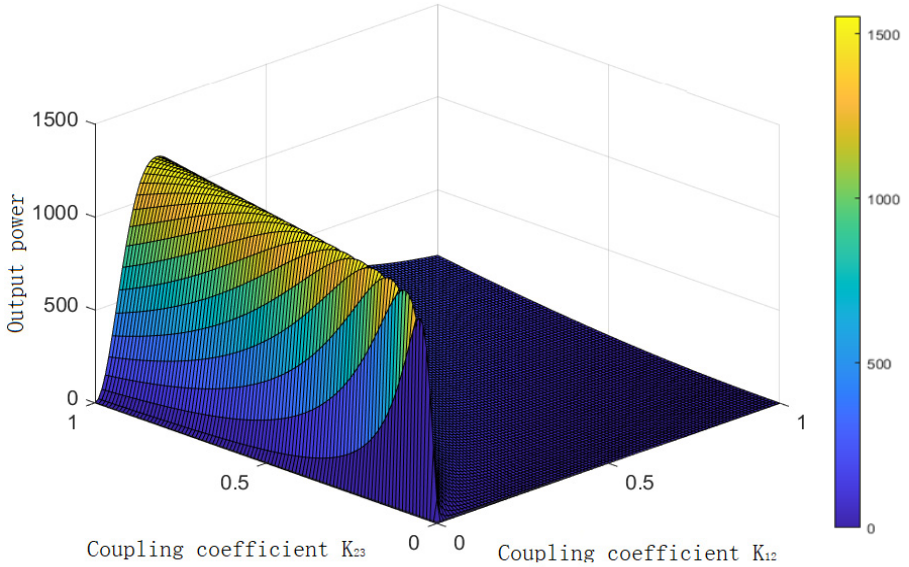

Figure 9. Relationship between output power and coupling coefficients k_{12} and k_{23}.

As Figure 9 shows, the output power would appear to peak with the increase in the coupling coefficient, and the output power would decrease with the increase in the coupling coefficient if the coupling coefficient continued to increase. Therefore, the output power did not increase with the increase in the coupling factor.

3.3.2. Influence of Coupling Coefficient on Transmission Efficiency

By substituting the coupling coefficient into the transmission efficiency formula, it had

$$\eta = \frac{\frac{\omega k_{12}^2 k_{23}^2 L^4 R_L}{R_2(R_3+R_L)+(\omega k_{23} L)^2}}{\times \frac{1}{\omega^2 k_{12}^2 L^2 (R_3+R_L)+(R_S+R_1)[R_2(R_3+R_L)+\omega^2 k_{12}^2 L^2]}} \quad (12)$$

Thus, the relationship between the coupling coefficient and the transmission efficiency could be obtained, as shown in Figure 10.

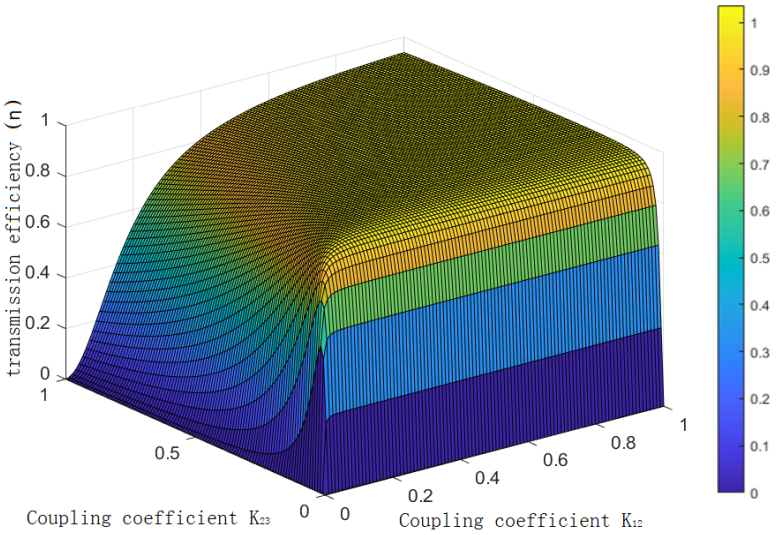

Figure 10. Relationship between transmission efficiency and coupling coefficients k_{12} and k_{23}.

It could be seen from Figure 10 that when other parameters were determined, the transmission efficiency of the system increased with the increase in the coupling coefficients k_{12} and k_{23}. Moreover, the influence of the coupling coefficient of the transmitting coil and the relay coil on the transmission efficiency of the system was slightly larger than that of the coupling coefficient of the relay coil and the receiving coil. Since the coupling coefficients k_{12} and k_{23} of the system had a certain negative correlation, it was difficult to make the transmission efficiency reach the maximum value. However, the transmission efficiency of the system would be improved with the increase in k_{12}.

3.3.3. Determination of Three-Coil Parameters

The three-coil WPT system designed in this paper was used for 110 kV transmission lines. According to the electric power industry standard of China—technical code for designing 110~500 kV overhead transmission line—the insulation distance standard of transmission lines under different voltage levels could be found.

It can be seen from Table 4 that the insulation distance of the 110 kV transmission line was 1.022 m. Therefore, 1.2 m was taken as the transmission distance of the designed coil.

Table 4. Insulation distance under different voltage levels.

Voltage Level (kV)	110	220	330	500
Single Insulator Thickness (mm)	146	146	146	155
Number of Insulator	7	13	17	25
Insulation Distance (m)	1.022	1.898	2.482	3.878

As the three-coil structure with a relay coil was used for power transmission, the position of the relay coil would affect the transmission performance of the system. In the three coils designed in this paper, the distance between the transmitting coil and the receiving coil was 1.2 m, and the relay coil was placed in the center of the transmitting coil

and the receiving coil. Three coils adopted the same planar spiral coil structure, and the coil parameters are listed in Table 5.

Table 5. Table of coil parameters.

Diameter of Wire (cm)	Coil Diameter (cm)	Outer Diameter of Coil (cm)	Number of Coils
0.2	20	32	20

The coil was modeled in Maxwell with the selected parameters, and the magnetic field intensity distribution of the coil is shown in Figure 11.

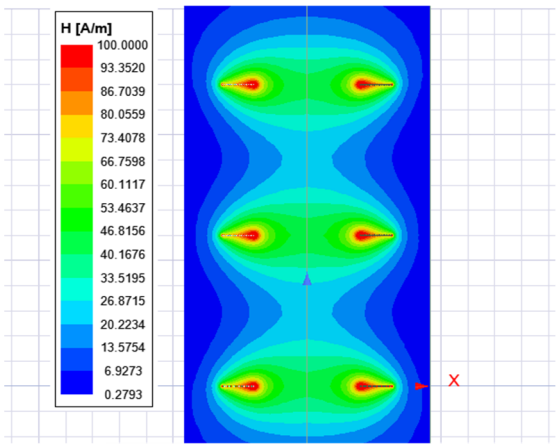

Figure 11. Magnetic field distribution of three coils.

3.3.4. Influence of Load Resistance on Transmission Performance

The mathematical model of the three-coil WPT system was modeled and analyzed in Maxwell. The coil diameter was 0.2 cm, the coil inner diameter was 20 cm, the coil outer diameter was 32 cm, and there were 20 coil turns. The self-inductance and mutual inductance of the simulation coil were $L_1 = L_2 = L_3 = L$ = 297.08 μH and $M_{12} = M_{23}$ = 10.315 μH, respectively. The coil resistance was $R_1 = R_2 = R_3 = R$ = 0.5 Ω, the input voltage U_S was =100 V, and the resonant frequency f was =100 kHz. Based on the above parameters, the load, output power, and transmission efficiency curves are shown in Figures 12 and 13.

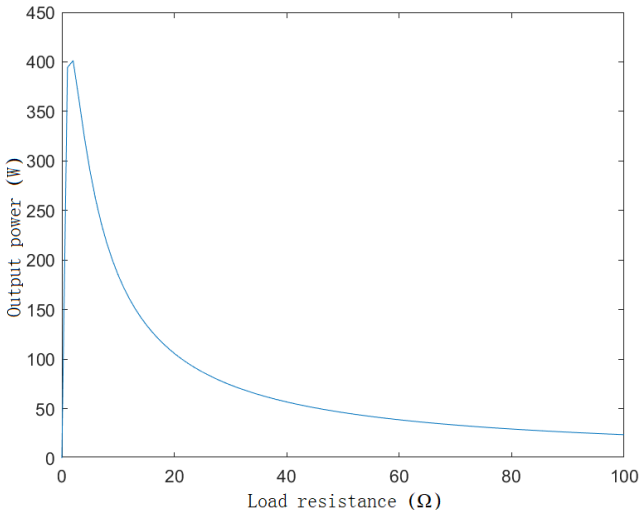

Figure 12. Relationship between output power and load resistance under the three coils.

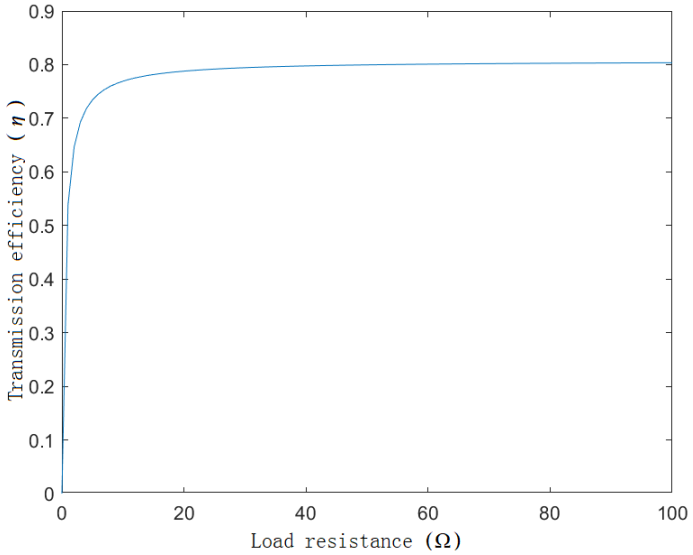

Figure 13. Relationship between transmission efficiency and load resistance under the three coils.

From Figure 12, it could be seen that the output power increased sharply with the increase in resistance. It decreased rapidly and, finally, the trends slowed down when it reached the peak value. It could be observed from Figure 13 that the transmission efficiency increased rapidly with the increase in resistance value when the resistance value was very small. It tended to be stable, reaching approximately 80% when the load resistance reached approximately 10 Ω.

4. Simulation

The current transformer was equivalent to an ideal voltage source through the above analysis and calculation. It was connected to an uncontrolled rectifier circuit and was filtered through the capacitance. Through the high-frequency inverter circuit, the direct current was transformed into an alternating current with a frequency of 100 kHz, and was connected to the three-coil system. Then, it was connected to a bridge rectifier circuit and capacitor filter. Finally, a 12 V voltage was output into the load through the Buck converter circuit. The simulation circuit is shown in Figure 14.

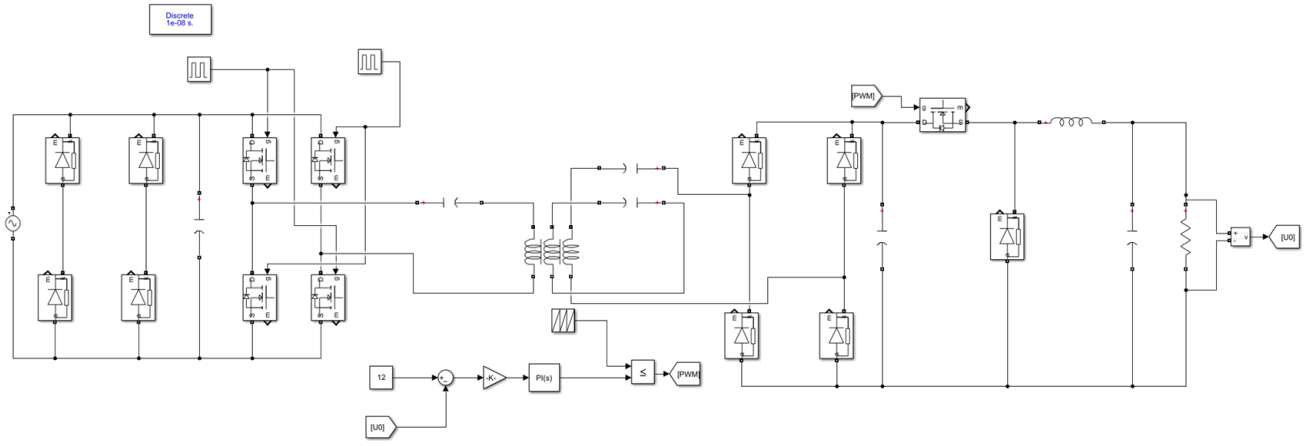

Figure 14. System simulation circuit.

Based on the above simulation parameters, the load resistance was set to be 10 Ω. The inverter output voltage, the receiving coil output voltage, and the system simulation output voltage waveforms were simulated, as shown in Figures 15–17.

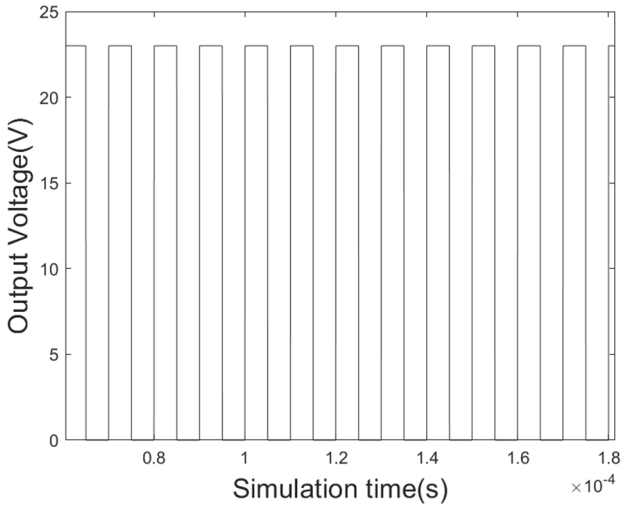

Figure 15. Voltage waveform of inverter output.

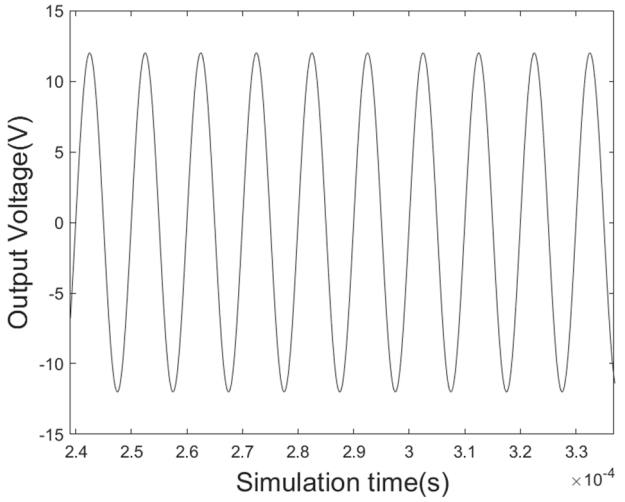

Figure 16. Voltage waveform of receiving coil output.

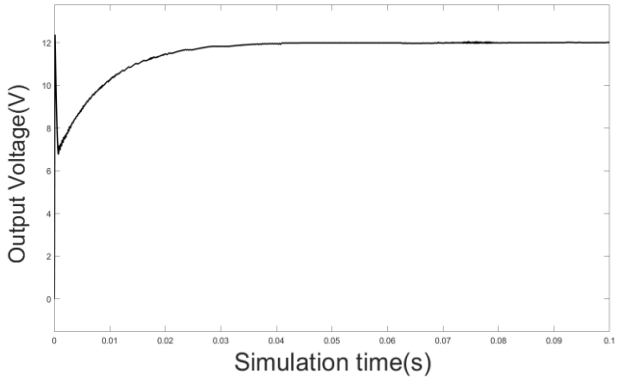

Figure 17. Voltage waveform of system simulation output.

It can be seen from Figures 15 and 16 that the system worked stably and could realize a normal WPT. As seen from Figure 17, the system output power was 14.4 W. As shown in Figure 18, at present, from the perspective of the monitoring functions, common online monitoring equipment for high-voltage transmission lines could basically be divided into the following categories: icing monitoring, line galloping, and wind deviation monitoring, lightning monitoring, insulator pollution monitoring, tower tilt monitoring, etc. Due to

the different energy consumptions of online monitoring devices with different functions, generally speaking, it was approximately 10 W, and the output power met the energy supply demand. Therefore, the system had practical application prospects.

(**a**). Dancing and pneumatic online monitoring equipment.

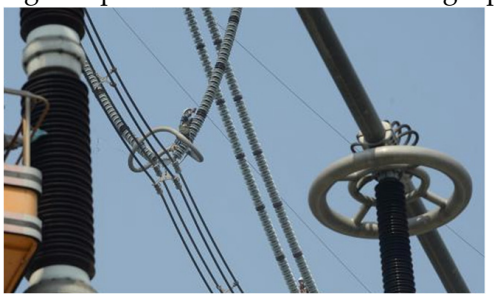

(**b**). Insulator pollution monitoring equipment.

(**c**). Icing online monitoring equipment.

Figure 18. Common high-voltage transmission line online monitoring equipment.

5. The Innovation of the Paper

1. This paper discussed a new power supply mode of online detecting equipment for high-voltage transmission lines, which included CT induction power extraction technology and three-coil WPT.
2. The designed method of the CT induction power extraction devices was presented, related parameters, such as the material structure of the iron core, were given, and the optimization was verified.
3. The three-coil system with a relay coil was analyzed theoretically and the energy efficiency effect of related parameters of the three-coil system was analyzed. Based on this, a three-coil WPT system was designed.

6. Comparative Analysis

Due to a lack of research on the combination of CT-induced energy harvesting and three-coil WPT, the following Table 6 only compared and analyzed CT-induced energy harvesting:

Table 6. Contrast table of CT-induced power extraction effect.

Reference	Magnetic Core Material Structure	Ability to Resist Saturation	Induced Voltage at Current 500 A
Reference [4]	C-core	Worse	7.931 V
Reference [5]	Permalloy	Worse	12 V
This article	Silicon steel, open-air gap structure	Magnetic saturation decreased	16.57 V

Through the above table, it could be concluded that through the design of the open-air gap of the iron core and the optimization of the related parameters, the antisaturation ability of the designed CT had a greater induction voltage of the energy-taking link. At the same time, in combining with the three-coil WPT technology, the system had a longer transmission distance. In addition, the system designed in this paper reduced the equipment's size and cost, increasing the system's stability and efficiency.

7. Conclusions

Focusing on the shortcomings of the battery life cycle in traditional battery power supply modes of high-voltage transmission line online monitoring devices, this paper proposed a way to realize an online power supply by combining induction power extraction technology with three-coil WPT technology. In this paper, the structure and parameters of the whole system were selected and optimized, and the correctness of the theoretical analysis was verified with simulation results. The research results showed that the proposed system had good theoretical significance and practical application value for the wireless online power supply of online monitoring devices of high-voltage transmission lines.

8. Patents

This section is not mandatory but may be added if there are patents resulting from the work reported in this manuscript.

Author Contributions: W.L. and Y.C. constructed the models and analyzed the parameter design methods. Y.C. carried out the simulations. W.L. and Z.P. developed a theoretical feasibility derivation. X.W. and C.X. carried out the background research and concept mapping. C.X. carried out the supervision. All authors have read and agreed to the published version of the manuscript.

Funding: This research was funded by the 2020 Anhui Provincial Natural Science Foundation Energy Internet Joint Fund Project (no. 2008085 UD14).

Data Availability Statement: No new data were created.

Conflicts of Interest: The authors declare no conflict of interest.

Notations

Symbol	Description	Unit
φ_m	the main magnetic flux	Wb
φ_{1m}	the leakage fluxes of the primary winding	Wb
φ_{2m}	the leakage fluxes of the secondary winding	Wb
φ_1	the main fluxes of the primary winding	Wb
φ_2	the main fluxes of the secondary winding	Wb
i_1	the current of the primary winding	mA
i_2	the current of the secondary winding	mA
N_1	the turns of the primary winding	-
N_2	the turns of the secondary winding	-
e_1	the potentials of the primary winding	V
e_2	the potentials of the secondary winding	V
E_2	the voltage effective value of the CT secondary side under no-load conditions	V
μ_r	the relative permeability of the magnetic core	H/m

μ_0	the vacuum permeability	H/m
l	the effective magnetic circuit length	m
S	the cross-sectional area of the iron core	m^2
f	the frequency of the transmission line current	Hz
I_1	the effective value of the transmission line current	mA
μ_{Fe}	the ferrum permeability	H/m
ω	the resonant angular frequency	r/s
M	the mutual inductance factor	H
R_1	the primary impedance	Ω
R_2	the secondary impedance	Ω
R_L	the load resistance	Ω
P_{max}	the expression of the maximum power	W
B_{max}	the maximum magnetic induction intensity	Wb/m^2
η	the transmission efficiency	-
P_{out}	the output power	W

References

1. Zhai, Y.; Sun, Y.; Dai, X.; Su, Y.; Wang, Z. Modeling and Analysis of Magnetic Resonance Mode Wireless Power Transfer System. *Chin. J. Electr. Eng.* **2012**, *32*, 155–160.
2. Jiao, B.; Fu, W.; Zhao, D. Design of CT energy source for high-voltage transmission lines. *Power Technol.* **2013**, *37*, 130–133.
3. Zhang, X. *Research on Multi-Coil Magnetic Coupling Resonant Wireless Power Transmission System*; North China Electric Power University: Beijing, China, 2019.
4. Rong, E. *Research on the Key Technology of Inductive Power Taking of Transmission Lines and Design of Power Taking Device*; Kunming University of Science and Technology: Kunming, China, 2019.
5. Wang, Y.; Yang, Z.; Li, S. Design of non-contact high-efficiency induction power-taking transformer for power cables. *Power Technol.* **2013**, *37*, 459–460+474.
6. He, X.; Wang, X. Design of high voltage line fault detection device. *Instrum. Technol. Sens.* **2015**, *12*, 32–35.
7. Zhuang, Y.; Xu, C.; Song, C.; Chen, A.; Lee, W.; Huang, Y.; Zhou, J. Improving Current Transformer-based energy extraction from AC power lines by manipulating magnetic field. *IEEE Trans. Ind. Electron.* **2019**, *67*, 9471–9479. [CrossRef]
8. Wang, W. *Research on Key Technologies of Wireless Energy Supply for High-Voltage Transmission Line Online Monitoring Device and System Optimization Design*; Southeast University: Nanjing, China, 2017.
9. Chen, C. *Optimization Analysis and Realization of High-Voltage CT Online Energy Harvesting Device*; Shandong University: Jinan, China, 2017.
10. Xie, Z.; Bi, T.; Jin, H.; Li, Y. Research on power supply of high-voltage transmission and distribution line online monitoring device. *Electr. Meas. Instrum.* **2016**, *53*, 16–21.
11. Vos, M.J. A Magnetic Core Permeance Model for Inductive Power Harvesting. *IEEE Trans. Power Electron.* **2020**, *35*, 3627–3635. [CrossRef]
12. Hou, J.; Wang, S.; Zhang, S.; She, Q.; Zhu, Y.; Li, C. Design and Application of a CT-Based High-Reliability Energy Harvesting Circuit for Monitoring Sensors in Power System. *IEEE Access* **2019**, *7*, 149039–149051. [CrossRef]
13. Liu, Z.; Li, Y.; Yang, H.; Na, D.; He, Z. An Accurate Model of Magnetic Energy Harvester in the Saturated Region for Harvesting Maximum Power: Analysis, Design and Experimental Verification. *IEEE Trans. Ind. Electron.* **2022**, *70*, 276–285. [CrossRef]
14. Long, M. *Research and Design of Power Supply System for High-Voltage Line Monitoring Device Based on Magnetic Resonance Coupling*; Wuhan University: Wuhan, China, 2018.
15. Huang, Z.; Zou, J.; Wang, Y.; Wang, L. Research on WPT technology based on relay coil and its application in high-voltage equipment. *J. Electrotech. Technol.* **2015**, *30*, 45–52.
16. Li, H. *Research on High Frequency Wireless Power Transmission Technology Based on Relay Coil*; Harbin Institute of Technology: Harbin, China, 2020.
17. Zhang, C.; Tang, N.; Zhong, W.; Lee, C.K.; Hui, R.S.Y. A new energy harvesting and wireless power transfer system for Smart Grid. In Proceedings of the 2016 IEEE 7th International Symposium on Power Electronics for Distributed Generation Systems (PEDG), Vancouver, BC, Canada, 27–30 June 2016.
18. Jiang, R.; Yan, S.; Deng, C.; Wang, Q.; Zhao, Y.; Tang, H.; Pan, J. Electric Field Analysis and Insulation Design of Wireless Power Transfer Coils Under High-Voltage Stress. In Proceedings of the 2022 IEEE International Conference on High Voltage Engineering and Applications (ICHVE), Chongqing, China, 25–29 September 2022.
19. Hou, X.; Su, Y.; Liu, Z.; Deng, Z. Wireless Power Transfer System of On-line Monitoring device for High Voltage Transmission Line Based on Double-sided LCC Resonant Network. In Proceedings of the 2021 IEEE PELS Workshop on Emerging Technologies: Wireless Power Transfer (WoW), San Diego, CA, USA, 1–4 June 2021; pp. 1–5.